PERGAMON

International Journal of Heat and Mass Transfer 44 (2001) 1573–1583

International Journal of HEAT and MASS TRANSFER

www.elsevier.com/locate/ijhmt

Revisiting heat transfer analysis for rapid solidification of metal droplets

Keh-Chin Chang *, Chih-Ming Chen

Department of Aeronautics and Astronautics, National Cheng-Kung University, Tainan 70101, Taiwan, ROC

Received 10 December 1999; received in revised form 25 May 2000

Abstract

There are two major mechanisms controlling the rapid solidification processing (RSP) of metal droplets in spray forming. One is the external extraction of heat which is usually carried out through convective and/or radiatively heat transfer modes. The other is the internal heat conduction combined with the nucleation-controlled solidification kinetics. Heat transfer analysis for the RSP of a metal droplet is revisited through the two modelings with and without consideration of internal heat conduction. Two test problems with cooling rates of metal droplets of 10^7 and 10^3 K/s are studied. Results through comparing the two predictions, obtained separately by the two investigated models, lead to the conclusion that the heat transfer modeling has to consider internal heat conduction in the RSP of metal droplets even with small Biot numbers. Other factors which affect the prediction accuracy in the work are discussed.

1. Introduction

The development of metastable structure by the rapid solidification processing (RSP) has received a great amount of study in the past [1] and continues to be an active subject of intensive research [2]. Among the RSP technology, spray forming (spray deposition, or spray casting) is a process whereby molten metal droplets are generated by atomization of a liquid metal stream and deposited on a subtrate [3]. It has been theoretically and experimentally shown that the rapid cooling (rates in the order of 10^3–10^7 K/s) of the small metal droplets (sizes of 10–10^3 μm) during transit to the substrate gives rise to fine grain (microstructually homogeneous) structure and, then, improves material properties (such as tensile strength, axial fatigue strength, fatigue crack growth resistance, superplasticity, etc.) over the conventional casting technology [3–5]. This is because very high cooling rates present in the spray forming process capture nonequilibrium state of metastable nature that cannot be done by the conventional casting technology. Accordingly, one of the important aspects of spray forming is that relating the heat-flow characteristics to the solidification behavior and resultant microstructure. A complete description of the RSP requires an additional regard of nucleation phenomena which is the initiation of solidification [6]. Once a critical nucleus has been formed, it will grow to a crystallite and start crystal growth process until the whole liquid metal becomes solid state. It is agreed that nucleation of crystal in liquid metal is the determining factor in the phase selection and the evolution of the solid microstructure [6–8].

There are four distinct regimes descriptive of the solidification process of a metal droplet in the flight to the substrate [4,5] as follows. In the first regime, cooling (without phase change) takes place until a nucleation temperature T_n is reached. As the metals in the liquid state are usually at high temperatures, both convective and radiative heat transfers have to be considered in the formulation. Due to the nonequilibrium nature of phase change in the RSP, T_n is lower than the melting (or solidification) temperature T_m of the metal which is equivalent to its equilibrium solid nucleation temperature. The difference $T_n - T_m$ is the undercooling in the solidification process. The second regime is recalescence

* Corresponding author. Tel.: +886-6-2757-575; fax: +886-6-2389-940.

E-mail address: kcchang@mail.ncku.edu.tw (K.-C. Chang).

0017-9310/01/$ - see front matter
PII: S0017-9310(00)00193-9

Nomenclature

Bi	Biot number, $h_c d/\lambda_i, i = 1$ or s
$(Bi)_{eff}$	effective Biot number, $(h_c + h_r)d/\lambda_i, i = 1$ or s
c	specific heat capacity
d	droplet diameter
ΔF_A	free energy of activation for transporting an atom across the liquid-crystal interface
h_c	convective heat transfer coefficient
h_p	Planck constant, 6.6256×10^{-34} J s
h_r	radiative heat transfer coefficient
I	nucleation rate
k	Boltzmann constant, 1.3806×10^{-23} J/K
L	latent heat
M	molecular weight
N	Avogadro's constant
n	number of atoms per unit volume
Nu	Nusselt number $(h_c d/\lambda_f)$
Pr	Prandtl number (v_f/α_f)
R	radius of droplet
r	radial coordinate
Ra	Rayleigh number $[(g\beta_f(T_d - T_\infty))/(v_f\alpha_f)]$
RSP	rapid solidification processing
T	temperature
t	time
ΔT_{max}	undercooling
Δt_c	time interval required for completion of phase change after recalescence
V	volume
v	moving velocity of the liquid–solid interface

Greek symbols

α	thermal diffusivity
β	thermal expansion coefficient
γ	interfacial free energy
ε	total hemispherical emissivity
λ	thermal conductivity
v	kinematic viscosity
ρ	density
σ	Stefan–Boltzmann constant, 5.669×10^{-8} W/m^2 K^4

Subscripts

d	droplet surface
f	film
l	liquid
m	melting
n	nucleation
s	solid
∞	environmental condition
0	initial condition

[6] in which there is a sudden release of latent heat within the droplet and part of the specimen is immediately heated to the recalescence temperature T_r. Here the solidification progresses extremely fast so that the crystallization of liquid metal can be assumed to begin with the onset of nucleation. Under the condition of very high cooling rates in the spray forming process, T_r is very close to the melting temperature and is usually assumed to be the same as T_m. After recalescence (the third regime), solidification continues to proceed but at a much slower rate until the solidification process is completed. In the last (fourth) regime, the droplet is now in solid phase and is cooled convectively and radiatively by the surrounding gaseous medium. The preceding description of the solidification process in spray forming indicates that, although the RSP is normally under heat transfer control, process analysis is further complicated by the degree to which kinetic factors can be responsible for departure from thermodynamic equilibrium. In other words, the key factors controlling the RSP of metal droplets include external extraction rate of heat and nucleation-controlled solidification kinetics.

It is obvious that a metal droplet can impact the substrate while in any of the four regimes described before. However, the partial solidification extent of a metal droplet prior to impact on the substrate is critical to the final formed microstructure [3,4,9]. If the partial solidification extent of the metal droplets arriving at the top surface of a deposit is too low, splashing and whipping up of liquid metal by the carrier gas produces pores of entrapped gas in the final product. On the other hand, excessive partial solidification depositing at the surface also leads to porous structure as insufficient molten metal is available to flow over the deposit to fill pores and interstices. Thus, the partial solidification extent of a metal droplet in the flight to the substrate is one of the key issues to be understood in the study of the spray forming.

Poulikakos and Waldvogel [5] made an extensive review on the transport phenomena aspects which are relevant to the process of spray forming. In accordance with this review paper, our knowledge based on the effects of transport phenomena in the spray forming technology is still very limited, because most of the existing studies were performed by material scientists and focus on metallurgical aspects of the process. For instances, due to a fact of small Biot numbers (<0.1) usually observed for the atomized metal droplets, a simple lumped model which does not account for heat conduction in the interior of metal droplet was adopted in most of the heat transfer analysis for cooling of a single metal droplet [10–14]. A typical justification for adopting this model approximation can be found from the study of Bayazitoglu and Cerny [15]. They analyzed the solidification processes of liquid metal droplets in powder production using a conventional lumped model

and a radially symmetric heat-condition model, but the modeling did not take into account the nonequilibrium phenomena of undercooled solidification which is a unique feature in the RSP. It was found that for relatively slow cooling rates up to 10^4 K/s, the lumped model was sufficiently accurate and the assumption of uniform temperature distribution inside the droplet justified. However, neglect of the nonequilibrium phenomena in the solidification process is a fatal defect in their analysis.

A complete numerical study on the fluid dynamics and convective (without radiative) heat transfer of a superheated liquid metal droplet, placed in a uniform, laminar gas stream, in the pre-solidification stage was performed by Megaridis [16], but the (nonequilibrium) solidification kinetics was not considered in the modeling either. The results improve our knowledge of the basic mechanisms of fluid dynamics and heat transfer in the laminar convective cooling of a liquid metal droplet. However, this approach cannot be applied directly to the real spray forming process due to two reasons. First, the relevant heat and fluid flow phenomena are often in the turbulent regime and must be combined with the nonequilibrium state of undercooled melt in solidification. Nevertheless, a comprehensive literature survey revealed that a study analogous to Megaridis [16] for liquid metal droplets in the turbulent regime and with the consideration of solidification kinetics is largely nonexistent so far in the published literature. The second and most important one is that a spray is constituted of a great number of droplets. It is, thus, numerically cost-ineffective by following the analyses analogous to Megaridis [16] for each droplet in the spray. Instead, interior head-conduction models combined with empirical correlations for the interfacial transport processes will be considered in this study.

In summary, there are two major mechanisms controlling the RSP of metal droplets in spray forming, that is, the external extraction of heat (convective and radiative heat transfer) and the internal heat conduction combined with the nucleation-controlled solidification kinetics. In recognition of this fact, a justification of the lumped models, which were conventionally used for the heat transfer analysis of metal droplets in the RSP by checking their values of the Biot number, needs to be re-examined. The simple problem of a single liquid metal droplet sitting in a quiescent environment, rather than the droplets in a spray, is considered here to fulfil this purpose. Since the extent of partial solidification prior to impact on the substrate is a key factor to control the final formed microstructure in spray-forming, special attention is placed on the capability of the model predictions for the undercooling, the time to recalescence, and the time interval required for the completion of phase change after recalescence.

2. Model formulation and analysis

2.1. Heat equation

Consider a spherically symmetrical droplet of liquid metal with uniform distribution of the initial temperature abruptly subjected to convective and radiative cooling on its surface. This heat conduction problem can be formulated as

$$\frac{1}{r^2}\frac{\partial}{\partial r}\left(r^2\lambda_i\frac{\partial T_i}{\partial r}\right)=\rho_i c_i\frac{\partial T_i}{\partial t},\quad i=\text{l or s}. \tag{1}$$

The boundary and initial conditions are specified by

$$\frac{\partial T}{\partial r}=0\quad \text{at } r=0,\ t>0, \tag{2}$$

$$-\lambda_i\frac{\partial T_i}{\partial r}=h(T_i-T_\infty)+\varepsilon_i\sigma(T_i^4-T_\infty^4)\quad \text{at } r=R, t>0,\ i=\text{l (before recalescence) or s (after recalescence)}, \tag{3}$$

$$T=T_0\quad \text{for } t=0,\ \text{in } 0\leqslant r\leqslant R. \tag{4}$$

The difference in the densities of liquid and solid phases at the interface during phase change gives rise to liquid motion across the interface. As a result, convective heat transfer driven by the internal flow circulation in the liquid phase has to be considered in the modeling and this complicates the problem much. Since the density changes for liquid and solid phases at the melting points for most metals are small (<10%), an assumption of $\rho_\text{l}=\rho_\text{s}$ is made in the work for the sake of simplicity. Thus, during phase change, there exists a solid–liquid interface in which two interfacial boundary conditions (at $r=r_\text{l}$) are needed as follows:

$$T_\text{l}=T_\text{s}, \tag{5}$$

$$-\lambda_\text{l}\frac{\partial T_\text{l}}{\partial r}+\rho_\text{l} vL=-\lambda_\text{s}\frac{\partial T_\text{s}}{\partial r}, \tag{6}$$

where

$$v=-\frac{\mathrm{d}r_\text{l}}{\mathrm{d}t}. \tag{7}$$

The lumped model assumes no temperature gradient within the droplet. The energy balance can then be formulated for the whole droplet as an entity by

$$-\rho_i c_i\left(\frac{4}{3}\pi R^3\right)\frac{\mathrm{d}T_i}{\mathrm{d}t}=4\pi R^2\left[h(T_i-T_\infty)+\varepsilon_i\sigma(T_i^4-T_\infty^4)\right],\quad i=\text{l or s}. \tag{8}$$

In the case of pure metals, the energy balance (during the period of phase change) is expressed by

$$\rho_\text{l} v(4\pi r_\text{l}^2)L=4\pi R^2\left[h(T_\text{s}-T_\infty)+\varepsilon_i\sigma(T_\text{s}^4-T_\infty^4)\right]. \tag{9}$$

2.2. Nucleation-controlled solidification kinetics

An extensive review on nonequilibrium solidification of undercooled metallic melts was made by Herlach [6]. For an undercooled droplet of liquid metal in spray forming, its kinetics of solidification can be reasonably assumed to begin with the onset of nucleation. A number of expressions have been proposed for the quasi-steady, homogeneous nucleation rate as a function of melt undercooling [6]. A typical form, based on classical nucleation theory, is given by [17]

$$I = \frac{nkT_l}{h_p}\exp\left(\frac{-\Delta F_A}{kT_l}\right)\exp\left[\frac{16\pi\gamma^3 T_m^2}{3k\rho_l^2 L^2 (T_m - T_l)^2 T_l}\right], \quad (10)$$

where the first exponential term in Eq. (10) expresses the ease with which atoms may diffuse through the melt to nucleus. Turnbull [17] found that the value of this exponential term was of the order of 10^{-2} at the solidification temperature in the RSP for most metals. Theoretical calculation of the interfacial free energy γ is usually difficult because the metastable nature of the undercooled melt precludes the measurement of the specific heat capacity at temperatures far removed from the equilibrium melt temperature T_m. Although few methods [18], based on Taylor series expansion of free energy centered at T_m, have been developed to obtain an expression of γ, these methods are restricted to the cases with small values of $\Delta T_{max}/T_m$. Thus, a value for γ can mostly be estimated through meaningful extrapolations and it is often difficult to examine such approximations. Turnbull [17] found the following relationship between the interfacial free energy and latent heat which was recursive from the experimental data of a number of homogeneous substances:

$$\gamma = A\frac{LM}{N^{1/3}(M/\rho_l)^{2/3}}. \quad (11)$$

Two classes of the above relationship were reported in the study of Turnbull [17]. One class which works for most of the metals, in particular the metals with cubic crystal structure together with mercury and tin, is specified by $A = 0.045$ with a standard deviation of 4.2%, while the other class which works for a small number of metals such as bismuth, antimony, germanium, etc. is specified by $A = 0.032$ with a standard deviation of 12.4%. More discussion on the reliability of the γ relationship of Eq. (11) is referred to [6,19].

On a basis of the classical nucleation theory, nucleation is expected in a volume V after a time t_n corresponding to the solution of

$$\int_V \int_0^{t_n} I(T_l)\,dt\,dV = 1. \quad (12)$$

Hirth [20] proposed another form of critical condition, on a statistical basis, in association with the lumped models to flag achievement of nucleation as

$$0.01\frac{VI(T_m - T_l)}{dT_l/dt} = 1. \quad (13)$$

2.3. Numerical method

The finite-volume method and the fourth-order Runge–Kutta method are used to solve iteratively the governing equations which are formulated using the interior heat conduction model (i.e., Eq. (1)) and the lumped model (i.e., Eqs. (8) and (9)), respectively. A grid mesh consisted of 100 uniformly distributed nodes is used in the time period before phase change for the calculations. After the phase change, totally 100 grid nodes are proportionally assigned to the liquid and solid portions in accordance with the ratios of r_l/R and $(R - r_l)/R$, respectively, at each time step. Uniformly distributed grid layouts are also adopted for each liquid or solid portion in the calculations after the phase change. The expression of Eq. (12) is calculated by summing instantaneous values of $I(T_l)$ over successive time increments. The point at which the sum reaches unity is flagged as a crystal nucleation event, and the corresponding values of time (t_n) and undercooling on the droplet's surface (for the interior heat conduction model) or in the entire volume (for the lumped model) are recorded.

When solving Eq. (1), fine enough grid mesh (100 radial nodes) is used to attain grid-independent solution. Iteration stops when the following convergent criterion is met:

$$\left|\frac{T^{i+1} - T^i}{T^i}\right| \leqslant 10^{-6}, \quad (14)$$

where the superscript denotes the ith iterate.

3. Test problems

Two experimental works with small droplets of pure liquid metals conducted by Turnbull and Cech [21] as well as Hofmeister et al. [22] are selected for the test problems. Turnbull and Cech [21] observed the solidification processes of a number of metal droplets on a microscope hot stage under a quiescent atmosphere of hydrogen or helium to avoid the formation of oxide film which may act as a heterogeneous nucleant and so give spuriously small undercoolings. Diameters of the liquid metal droplets in the experiments of Turnbull and Cech [21] ranged from 10 to 100 μm. As reported by Turnbull and Cech [21], the errors for the measurements of undercooled temperatures due to the uncertainties in use of thermocouple were estimated to be ±5%. Table 1 summarizes the measured results for the undercoolings [21] and the values of the corresponding interfacial free

Table 1
Results of the observed undercooling and the derived interfacial free energy by Turnbull and Cech [17,21]

Metal	Melting point T_m (K)	Droplet size d (μm)	Atmosphere	Undercooling $\Delta T_{max}/T_m$ (%)	Interfacial free energy γ (mJ/m^2)
Bismuth (Bi)	544	10–50	H_2	16.6	54.4
Lead (Pb)	600.7	10–50	H_2	15.1	33.3
Antimony (Sb)	903	15–30	H_2	15.0	101
Aluminum (Al)	931.7	50–100	H_2	14.0	54.5
Silver (Ag)	1233.7	20–40	He	18.4	126
Gold (Au)	1336	20–50	He	17.2	132
Copper (Cu)	1356	15–50	He or H_2	17.4	177
Nickel (Ni)	1726	50–100	He	18.5	255
Cobalt (Co)	1763	20–50	He	18.7	234
Iron (Fe)	1803	30–100	He	16.4	204
Palladium (Pd)	1828	30–100	He	18.2	209

energy derived from the measured undercooling data by Turnbull [17] for a number of metals.

In view of the test condition investigated by Turnbull and Cech [21], the external heat extraction was performed through natural convection and thermal radiation. The heat transfer coefficient due to natural convection h is evaluated using the empirical formula [23] of

$$Nu = \left[\left(2 + \frac{0.589 Ra^{1/4}}{\left[1 + (0.492/Pr)^{9/16} \right]^{4/9}} \right)^6 + (\overline{c_i} Ra^{1/3})^6 \right]^{1/6} \quad \text{for } 10 \leqslant Ra \leqslant 2 \times 10^9, \tag{15}$$

where the $\overline{c_i}$ value correlated with various Prandtl numbers can be found in Table 3A of [23]. It is noted that the thermophysical properties of the surrounding fluid required for determining the values of Nu, Pr, and Ra are evaluated at the film temperature T_f which is defined by $T_f = (T_d + T_\infty)/2$.

Hofmeister et al. [22] conducted a series of undercooling experiments using a drop tube facility which was operated in a near vacuum (with vacuum level of 1×10^{-5} Torr), microgravity (10^{-6} g) environment. Thus, the h value shown in Eqs. (3), (8) and (9) is set to be zero in the calculations for this test problem. The Biot number, which provides a measure of the internal conduction resistance relative to the external heat transfer resistance, is conventionally applicable to the conduction problems that involve surface convection effects, i.e., $Bi = h_c d/\lambda$. Nevertheless, an effective Biot number can be defined by using the combined heat transfer coefficient $(h_c + h_r)$, in which the radiative heat transfer coefficient is given by

$$h_r = \varepsilon\sigma \frac{T_i^4 - T_\infty^4}{T_i - T_\infty}, \quad i = \text{l or s}. \tag{16}$$

Clearly, the effective Biot number for this test problem becomes $Bi = h_r d/\lambda$. Larger (in the order of 10^3 μm) and monodispersed droplet sizes of pure liquid metals were investigated. Observations of the recalescence and solidification events were made using the silicon dioxide infrared detectors. These detectors recorded the changes in brightness that accompanied recalescence and solidification of undercooled metal droplets. As reported by Hofmeister et al. [22], the detector output gave the time of radiant cooling from release to solidification with an uncertainty of ±30 ms. No direct temperature measurements were made in the experiment. The nucleation temperature T_n was inversely calculated from the time history of the brightness with an assumption of uniform droplet temperature during the experiment. The errors in undercooling calculations were estimated to be about ±50 K. Table 2 summarizes the measured results for the undercoolings and the average times to recalescence (t_n) for a number of metals in the study of Hofmeister et al. [22]. Information of the interfacial free energy for the metals listed in Table 2 is estimated by means of the empirical formula of Eq. (11). Both cases of $A = 0.045$ and 0.032 were tested in this work and the results predicted with the case of $A = 0.045$ were found in better agreement with the measured data than with $A = 0.032$ for all the metals shown in Table 2. Therefore, the γ values estimated through Eq. (11) with $A = 0.045$ are suggested and listed in Table 2.

No information of the initial droplet temperatures was provided in both the experiments. Ten percent higher than the melting temperature for each investigated metal is assumed as the initial temperature of the liquid metal droplet in the following calculations. An accurate calculation of nonequilibrium solidification phenomena requires a confident knowledge of thermophysical properties such as the specific heat capacity, thermal conductivity, emissivity, etc. in the metastable regime of an undercooled melt. So far, only scarce information is available on such properties in the equilibrium liquid state above the melting temperature, but almost nothing is known about thermophysical parameters and their temperature dependence in the

Table 2
Results of the measured time to recalescence and the estimated undercooling by Hofmeister et al. [22]

Metal	Melting point T_m (K)	Droplet size d (mm)	Time to recalescence $t_n \pm 0.03$ (s)	Undercooling $(\Delta T_{max} \pm 50)/T_m$ (%)	Interfacial free energy[a] γ (mJ/m^2)
Titanium (Ti)	1939	1.8	4.5	18.0 ± 2.6	212
Platinum (Pt)	2045	2.6	3.0	18.6 ± 2.4	266
Zinconium (Zr)	2125	5.0	3.5	20.2 ± 2.4	188
Rhodium (Rh)	2233	2.3	3.2	20.2 ± 2.2	283
Hafnium (Hf)	2500	4.6	2.2	18.0 ± 2.0	237
Niobium (Nb)	2740	4.4–5.6	2.1–2.8	17.5 ± 1.8	264
Molybdenum (Mo)	2897	4.9	2.6	17.9 ± 1.7	291
Tantalum (Ta)	3287	3.7	1.3	19.8 ± 1.5	341

[a] The interfacial free energy is estimated by means of the empirical formula of Eq. (11) with $A = 0.045$.

metastable regime of an undercooled melt [6]. Thus, the thermophysical properties for each investigated metal are assumed to be temperature-independent and evaluated at its melting temperature. Table 3 summarizes the material properties necessary in the calculations. The emissivity of liquid metals is a property which is usually measured less accurately than the other thermophysical properties. The sources of experimental data for ε_l are very limited, and furthermore, data for ε_l of undercooled melts are nonexistent. Therefore, solid emissivity values are used for both the liquid and solid phases where available. No experimental data of the thermal conductivity of liquid phase, λ_l, for palladium, titanium, rhodium, hafnium, and molybdenum are found. For lack of available data, same values of λ_s are used for λ_l for these metals in the following calculations.

4. Results and discussion

Hereinafter, the model considering internal heat conduction, i.e., Eqs. (1)–(7), is called Model 1, while the lumped model, i.e., Eqs. (8) and (9), is called Model 2. Fig. 1 presents typical variations of surface temperature vs time for a liquid nickel droplet of $d = 100$ μm obtained individually with Models 1 and 2. The surface temperature of the liquid nickel droplet drops quickly below its melting point (1726 K) without phase change until the nucleation temperature T_m is reached. The phase change is then occurred immediately and accompanied with a sudden release of latent heat, which in turn raise the surface temperature up to the melting point of nickel. Fig. 2(a) and (b) presents the internal temperature distributions at the times before and after

Table 3
Material properties [25–28]

Metal	M (g/mol)	L (J/kg)	ρ_l (kg/m^3)	c_l (J/kg K)	c_s (J/kg K)	λ_l (W/m K)	λ_s (W/m K)	ε
Bi	208.98	54,058	10,068	145.86	142.71	12.4	7.61	0.10
Pb	207.20	23,021	10,678	148.03	141.94	15.5	31.2	0.63
Sb	121.75	163,236	6483	257.74	254.44	25.9	16.7	0.59
Al	26.98	396,968	2385	1176.64	1259.88	90.7	211	0.15
Ag	107.87	104,730	9346	310.30	296.94	175	355	0.05
Au	196.97	63,726	17,360	157.19	169.78	105	247	0.129
Cu	63.55	206,748	8000	516.85	526.75	166	330	0.105
Ni	58.71	297,700	7905	734.28	616.66	82.5	90.0	0.21
Co	58.93	274,756	7760	687.24	647.45	99.2	40.0	0.36
Fe	55.85	247,229	7015	824.11	761.96	40.3	34.6	0.36
Pd	106.40	165,007	10,490	326.32	333.85	–[a]	75.5	0.25
Ti	47.90	295,447	4110	742.48	741.02	–[a]	28.4	0.36
Pt	195.09	100,805	19,000	178.01	179.70	91.3	103.7	0.30
Zr	91.22	229,326	5800	458.67	394.35	31.8	31.9	0.30
Rh	102.90	208,824	10,800	406.57	383.93	–[a]	94.3	0.196
Hf	178.49	134,786	11,100	187.53	206.28	–[a]	24.1	0.327
Nb	92.91	283,814	7830	360.26	380.18	81.5	88.0	0.27
Mo	95.94	407,536	9340	420.57	573.90	–[a]	80.9	0.325
Ta	180.95	174,807	15,000	231.22	266.41	66.5	66.6	0.28

[a] No available data are found. Same value as λ_s is used in the calculations.

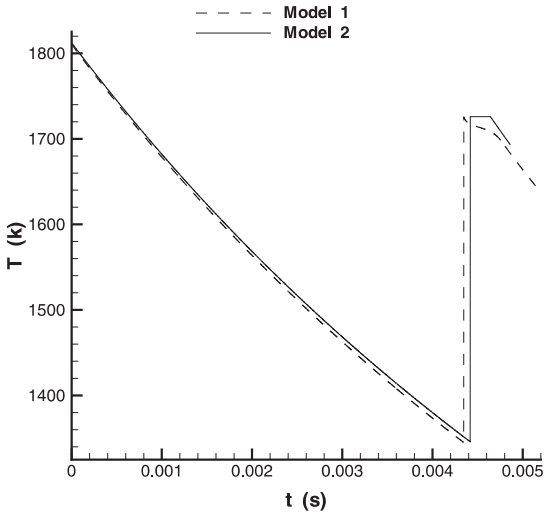

Fig. 1. Variations of surface temperature vs time for nickel droplet with $d = 100$ μm using Models 1 and 2 (with and without consideration of internal heat conduction, respectively).

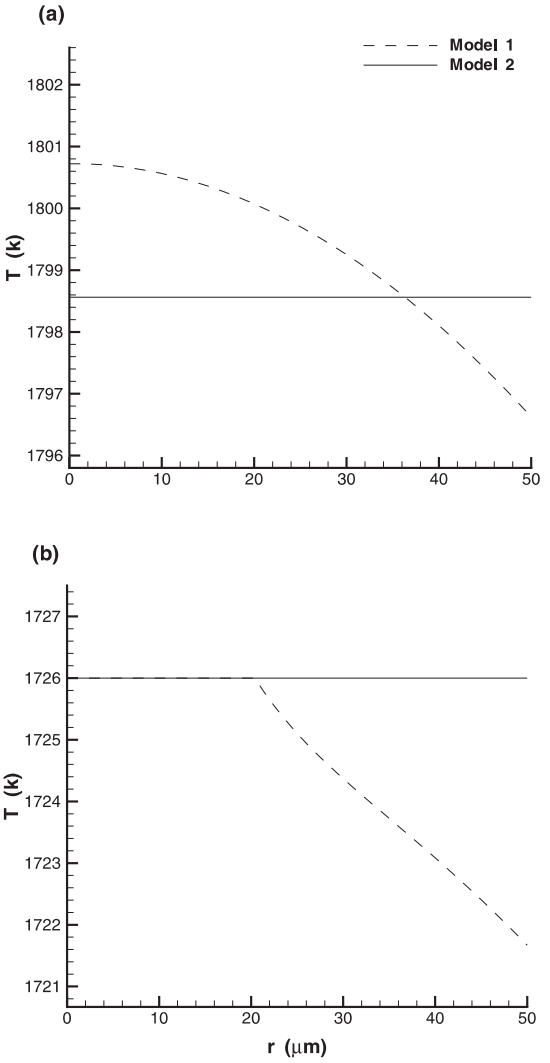

Fig. 2. Temperature distributions at (a) $t = 9.9 \times 10^{-4}$ s (before recalescence) and (b) $t = 4.56 \times 10^{-3}$ s (after recalescence) for nickel droplet with $d = 100$ μm using Models 1 and 2 (with and without consideration of internal heat conduction, respectively).

recalescence. Although there exists an observable temperature variation inside the nickel droplet in the solution obtained with Model 1, the undercooling extents and T_ms predicted between the two models differ slightly. This implies that the internal heat conduction can be reasonably neglected in the calculation before recalescence when the Biot number is small (<0.1). After recalescence, the release of latent heat in the interface of liquid and solid phases leads to the thermal energy built-up at the solidification front and the development of temperature gradient across the solid portion of the droplet in the calculation using Model 1. In contrast, the release rate of latent heat from the solidification front to the droplet surface is assumed to be infinitely fast by Model 2. The apparently different release rates of latent heat from the solidification front to the droplet surface determined, respectively, by these two models result in the remarkable difference in predicting the time to the completion of solidification t_s, which will be presented later.

Since a number of metal droplets with various sizes (see Table 1) were observed at one time in the experiment of Turnbull and Cech [21], the reported undercoolings were the averaged results for a group of various-size droplets. It is well agreed that the undercooling at the oneset of nucleation increases with the decreasing droplet size of liquid metal [11]. The droplet sizes with the lower and upper bounds listed in Tables 1 and 2 are thus calculated using both the models. Table 4(a) and (b) lists the predicted and measured undercooled extents under the atmospheres of hydrogen and helium, respectively, for the test problem experimentally investigated by Turnbull and Cech [21]. Table 5 lists similar results but for the test problem experimentally investigated by Hofmeister et al. [22]. Tables 6 and 7 list the times to recalescence t_n and the time intervals required for the completion of phase change after recalescence Δt_c, predicted with the two heat-transfer models, for the test problems of Turnbull and Cech [21] as well as Hofmeister et al. [22], respectively. Here Δt_c is equal to $t_s - t_n$ in which t_s is the time when $r_l = 0$. No available measured data, except for t_n in the test problem of Hofmeister et al. [22], can be used as the comparison basis for the predictions shown in Tables 6 and 7.

Table 4
Comparison of the undercooled extent in the (a) H_2 and (b) He environments for the test problem of Turnbull and Cech [21]

Metal droplet sizes (μm)	Biot number ($\times 10^3$)		Undercooled extent, $\Delta T_{max}/T_m$ (%)		
	Bi	$(Bi)_{eff}$	Experimental data [21]	Predictions by Model 1	Predictions by Model 2
(a) H_2 environment					
Bi 10–50	40.57–41.01	40.57–41.01	16.6 ± 0.8	20.45–18.63	20.38–18.53
Pb 10–50	34.40–34.77	34.41–34.80	15.1 ± 0.8	17.79–16.22	17.68–16.12
Sb 15–30	26.41–26.50	26.42–26.53	15.0 ± 0.8	18.56–17.81	18.46–17.71
Al 50–100	7.75–7.82	7.75–7.82	14.0 ± 0.7	16.78–16.19	16.75–16.15
Cu 15–50	5.35–5.38	5.35–5.38	17.4 ± 0.9	23.03–21.48	23.01–21.45
(b) He environment					
Ag 20–40	4.02–4.04	4.02–4.04	18.4 ± 0.9	24.13–23.16	24.11–23.13
Au 20–50	7.05–7.08	7.05–7.08	17.2 ± 0.9	21.46–20.36	21.42–20.32
Cu 15–50	4.50–4.52	4.50–4.52	17.4 ± 0.9	23.00–21.44	22.97–21.41
Ni 50–100	10.63–10.68	10.65–10.73	18.5 ± 0.9	22.89–22.08	22.85–22.02
Co 20–50	8.95–8.99	8.96–9.02	18.7 ± 0.9	24.70–23.43	24.66–23.38
Fe 30–100	22.42–25.58	22.47–25.60	16.4 ± 0.8	20.53–19.27	20.42–19.15
Pd 30–100	12.04–12.12	12.06–12.20	18.2 ± 0.9	23.86–22.33	23.80–22.27

Table 5
Comparison of the undercooled extent for the test problem of Hofmeister et al. [22]

Metal droplet sizes (mm)	Biot number $(Bi)_{eff} \times 10^6$	Undercooled extent, $\Delta T_{max}/T_m$ (%)		
		Experimental data [22]	Predictions by Model 1	Predictions by Model 2
Ti 1.8	7.03	18.0 ± 2.6	15.20	15.14
Pt 2.6	2.83	18.6 ± 2.4	17.39	17.37
Zr 5.0	17.4	20.2 ± 2.4	17.45	17.35
Rh 2.3	2.03	20.2 ± 2.2	17.39	17.37
Hf 4.6	36.6	18.0 ± 2.0	17.44	17.27
Nb 4.4–5.6	11.1–14.2	17.5 ± 1.8	17.28–17.17	17.21–17.08
Mo 4.9	15.6	17.9 ± 1.7	20.78	20.69
Ta 3.7	19.9	19.8 ± 1.5	17.45	17.33

Both values of the conventional (considering surface convection only) and effective (considering both surface convection and radiation) Boit numbers for the cases investigated by Turnbull and Cech [21] are summarized in Table 4. The differences between Bi and $(Bi)_{eff}$ are less than 0.4%. It means that the surface convection is the dominant process for the cooling of the metal droplets in the test problem of Turnbull and Cech [21]. The effective Biot numbers (consisted of surface radiation only) for the cases investigated by Hofmeister et al. [22] are summarized in Table 5. All values of the conventional and effective Biot numbers listed in Table 4 are in order of 10^{-2}–10^{-3}, while of the effective Biot numbers listed in Table 5 are in order of 10^{-5}–10^{-6}. Note that the lumped model is conventionally thought to be a proper approximation for the heat transfer analysis with $Bi < 0.1$. The following observations are made from the comparison between the two predictions using Models 1 and 2 as shown in Tables 4–7. First, the choice of either Model 1 (with consideration of internal heat conduction) or Model 2 (without consideration of internal heat conduction) in the formulation makes slight differences in the predictions of the undercooled extent $(\Delta T_{max}/T_m)$ and the time to recalesence for all the investigated metals. In contrast, the lumped model which neglects internal heat conduction (Model 2) yields remarkable underestimations of the time intervals required for the completion of phase change after recalescence, as compared to the model considering internal heat conduction (Model 1). It is known that the extent of partial solidification prior to impact on the substrate is a key factor to control the final formed microstructure in the spray forming process [4,9]. This implies that a flying droplet is anticipated to arrive at the substrate at a certain time within $t_n \pm \Delta t_c/2$. Thus, accurate predictions of t_n and Δt_c are important in the simulation of the RSP of a liquid metal droplet. Effect of atmospheric fluid on the undercooling can be studied by comparing the two RSP

Table 6
Comparison of the time to recalescence (t_n) and the time interval required for completion of phase change after recalescence (Δt_c) in the (a) H_2 and (b) He environments for the test problem of Turnbull and Cech [21]

Metal droplet sizes (μm)	Model 1		Model 2		Discrepancy $t[1-(\Delta t_c)_2/(\Delta t_c)_1]\times 100\%$
	$(t_n)_1\times 10^4$ (s)	$(\Delta t_c)_1\times 10^4$ (s)	$(t_n)_2\times 10^4$ (s)	$(\Delta t_c)_2\times 10^4$ (s)	
(a) H_2 environment					
Bi 10–50	0.365–8.02	0.553–14.14	0.373–8.21	0.477–12.22	13.7–13.6
Pb 10–50	0.283–6.31	0.120–3.34	0.289–6.46	0.100–2.80	16.7–16.2
Sb 15–30	0.382–1.46	0.833–3.36	0.391–1.49	0.735–2.97	11.8–11.6
Al 50–100	6.17–23.63	5.35–21.79	6.33–24.24	4.90–20.00	8.41–8.21
Cu 15–50	0.779–7.97	0.171–2.31	0.799–8.18	0.146–1.98	14.6–14.3
(b) He environment					
Ag 20–40	1.326–5.05	0.155–0.771	1.360–5.18	0.125–0.636	19.4–17.6
Au 20–50	1.103–5.96	0.349–2.41	1.308–6.11	0.304–2.13	12.9–11.6
Cu 15–50	0.919–9.40	0.204–2.73	0.942–9.64	0.174–2.37	14.7–13.2
Ni 50–100	11.43–43.20	0.710–4.21	11.62–44.30	0.300–2.23	57.7–47.0
Co 20–50	1.785–10.39	0.0–0.0	1.830–10.65	0.0–0.0	0.0–0.0
Fe 30–100	3.479–35.64	0.0–0.0	3.562–36.50	0.0–0.0	0.0–0.0
Pd 30–100	2.413–24.61	0.375–5.36	2.472–25.03	0.241–4.01	35.7–25.2

Table 7
Comparison of the time to recalescence (t_n) and the time interval required for the completion of phase change after recalescence (Δt_c) for the test problem of Hofmeister et al. [22]

Metal droplet sizes (mm)	Measurements [22] $t_n\pm 0.03$ (s)	Model 1		Model 2		Discrepancy $[1-(\Delta t_c)_2/(\Delta t_c)_1]\times 100\%$
		$(t_n)_1$ (s)	$(\Delta t_c)_1$ (s)	$(t_n)_2$ (s)	$(\Delta t_c)_2$ (s)	
Ti 1.8	4.5	1.55	0.45	1.59	0.33	26.7
Pt 2.6	3.0	2.98	1.21	3.05	0.96	20.7
Zr 5.0	3.5	4.03	0.92	4.11	0.84	8.7
Rh 2.3	3.2	4.02	0.93	4.12	0.77	17.2
Hf 4.6	2.2	1.63	0.99	1.66	0.64	35.4
Nb 4.4–5.6	2.1–2.8	1.93–2.43	0.96–1.28	1.97–2.48	0.76–0.98	30.8–23.4
Mo 4.9	2.6	2.67	1.28	2.72	0.92	28.1
Ta 3.7	1.3	1.13	0.37	1.15	0.22	40.5

results of copper droplets, which are separately obtained under hydrogen and helium atmospheres (see Table 4(a) and (b), respectively). Only slight differences in the undercoolings predicted separately under these two different atmospheres are observed for both the tested models. This observation is consistent with the measured results of Turnbull and Cech [21] in which the same value of undercooling was reported for both the cases under hydrogen and helium atmospheres. Nevertheless, approximately 20% differences in the predictions of t_n and Δt_c are found between these two different atmospheres. This shows that the determination of t_n and Δt_c is more parameter-sensitive than the determination of undercooling in the calculations.

Comparisons between the predicted and measured undercooled extents for both the test problems (cf. Tables 4 and 5) reveal that the predictions made for the test problem of Turnbull and Cech [21] (small droplets under atmosphere) are overestimated, while the predictions made for the test problem of Hofmeister et al. [22] (relatively large droplets in near vacuum environment) are in better agreement with, as compared to the other test problem, the experimental results. External heat extraction from a metal droplet is accomplished by natural convection and thermal radiation for the test problem of Turnbull and Cech [21]. The typical values for the terms of $h_c(T_i - T_\infty)$ and $\varepsilon_l\ \sigma(T_l^4 - T_\infty^4)$ are in order of magnitude of 10^9 and 10^5, respectively. This is because the Nu values evaluated by Eq. (15) are slightly larger than 2 for all the cases summarized in Table 1 and it leads to, according to the definition of Nu, $h_c \propto 1/d$. Thus, the contribution to the external heat extraction from thermal radiation can be neglected in the test problem of Turnbull and Cech, whereas thermal radiation is the only route to extract heat from the metal droplets in the test problem of Hofmeister et al. [22]. Substituting these typical values of $h_c(T_i - T_\infty)$ and $\varepsilon_l\ \sigma(T_l^4 - T_\infty^4)$ into Eq. (8), the cooling rates for the test

problems of Turnbull and Cech as well as Hofmeister et al. are estimated in order of magnitude of 10^7 and 10^3 K/s, respectively. With the cooling rates as high as 10^7 K/s, deeply undercooled state was reached for all the melts in the test problem of Turnbull and Cech [21]. This inference can be further corroborated by the occurrence of the hypercooled state, in which the undercooled extent is so deep so that the whole melt is immediately converted to the solid state at recalescence, for the cobalt and iron droplets as shown in Table 4(b). It was reported [8,24] that some modifications accounting for transient effects have to be included in the expression of nucleation rate for deeply undercooled melts. The present overestimations of the undercoolings for the test problem of Turnbull and Cech may stem from the neglect of transient effects in the nucleation rate; and this inference remains to be studied further. Nevertheless, the quasi-steady relationship given by Eq. (10) is useful in estimation of the nucleation rates for the test problem of Hofmeister et al. in which the cooling rates are relatively slow.

As reported in Tables 2 and 3, the thermophysical properties of some thermal conductivity for liquid λ_l and all the interfacial free energy γ used for the calculations in the test problem of Hofmeister et al. are known with less confidence than those in the test problem of Turnbull and Cech. Moreover, errors in the estimation of the total hemispherical emissivity for the liquid become more influential to the calculations made for the test problem of Hofmeister et al., because the radiative transfer mode is now the only route for external cooling, than for the other test problem. Therefore, more errors are brought in the solutions of the RSP for the liquid metal droplets in the test problem of Hofmeister et al. A comparison made between the predicted and measured times to recalescence (see Table 7) shows remarkable differences for some metals such as titanium, rhodium, etc. which could be due to the use of the less accurate thermophysical properties in the calculations. In contrast to t_n, the predicted undercooled extents are in satisfactory agreement with the experimental data. As mentioned before, this is because the determination of undercooling ΔT_{max} is less parameter-sensitive than the determination of t_n in the RSP calculations. However, improvement in the predictions for the test problem of Hofmeister et al. has to wait for the availability of more reliable thermophysical properties summarized in Tables 2 and 3.

5. Conclusions

Heat transfer analysis for the RSP of a liquid metal droplet is re-examined with and without consideration of internal heat conduction in the droplets (Models 1 and 2, respectively). Two test problems with the cooling rates of metal droplets in order of magnitude of 10^7 and 10^3 K/s, which are closer to the upper and lower extremes of the cooling rates in the spray forming process, investigated, respectively, by Turnbull and Cech [21] and Hofmeister et al. [22] are studied. Note that the Bi values for the test problem of Turnbull and Cech are as low as 10^{-2}–10^{-3}. Comparative studies made between the two tested heat transfer models show that Model 2 yields remarkable underestimations of the time interval required for the completion of phase change after recalescence Δt_c, which is an important parameter determining the extent of partial solidification in the RSP, as compared to Model 1. In contrast to the Δt_c prediction, the lumped model (Model 2) can yield closer predictions for the undercooling and time to recalescence as does Model 1. Overall the heat transfer modeling has to consider heat conduction inside metal droplet for the RSP in spray forming.

For the fast cooling rates of 10^7 K/s such as in the test problem of Turnbull and Cech, transient effects on the nucleation rates may have to be considered in the modeling due to the resultant deeply undercooled melts. This issue remains to be studied further.

Finally, lack of reliable thermophysical properties of the investigated metals such as $\varepsilon_l, \lambda_l, \gamma$ prevents accurate solutions from the present calculations. Improvement in the theoretical solution has to wait for the availablity of more reliable thermophysical properties, including such in the metastable regime of undercooled melts which are almost nonexistent at the present time. In addition, this study simplified the RSP of a metal droplet by using a spherically symmetrical (one-dimensional) model formulation, which is physically not correct in the simulation of the test conditions of Turnbull and Cech [21]. The natural convective cooling makes a multidimensional analysis necessary and this remains to be studied further.

Acknowledgements

The authors gratefully acknowledge the grant support from the National Science Council of the Republic of China under the contract NSC 87-2212-E006-073.

References

[1] H. Jones, Rapid Solidification of Metals and Alloys, Institution of Metallurgists, London, UK, 1982.
[2] L.A. Jacobson, J. Mckittrick, Rapid solidification processing, Mater. Sci. Eng. R11 (1994) 355–408.
[3] E.J. Lavernia, N.J. Grant, Spray deposition of metals: a review, Mat. Sci. Eng. 98 (1988) 381–394.
[4] E.J. Lavernia, The evolution of microstructure during spray atomization and deposition, Int. J. Rapid Solidification 5 (1989) 47–85.

[5] D. Poulikakos, J.M. Waldvogel, Heat transfer and fluid dynamics in the process of spray deposition, in: D. Poulikakos (Ed.), Advances in Heat Transfer, vol. 28, Academic Press, London, UK, 1996, pp. 1–74.
[6] D.M. Herlach, Non-equilibrium solidification of undercooled metallic melts, Mater. Sci. Eng. R12 (1994) 179–272.
[7] W.T. Kim, D.L. Zhang, B. Cantor, Nucleation of solidification in liquid droplets, Metall. Trans. A 22 (1991) 2487–2501.
[8] J.H. Perepezko, M.J. Uttormark, Nucleation-controlled solidification kinetics, Metall. Mater. Trans. A 27 (1996) 533–547.
[9] S. Annavarapu, D. Apelian, A. Lawley, Spray casting of steel strip : process analysis, Metall. Trans. A 21 (1990) 3237–3256.
[10] E. Gutierrez-Miravete, E.J. Lavernia, G.M. Trapaga, J. Szekely, N.J. Grant, A mathematical model of the spray deposition process, Metall. Trans. A 20 (1989) 71–85.
[11] P.S. Grant, B. Cantor, L. Katgerman, Modelling of droplet dynamic and thermal histories during spray forming – I. Individual droplet behavior, Acta Metallurgica et Materialia 41 (1993) 3079–3108.
[12] J.K. McCoy, A.J. Markworth, E.W. Collings, R.S. Brodkey, Cooling and solidification of liquid-metal drops in a gaseous atmosphere, J. Mater. Sci. 27 (1992) 761–766.
[13] F. Folio, A. Lacour, Heat transfer by conduction and convection between a spherical droplet particle and a two-phase fluid, Int. J. Rapid Solidification 9 (1996) 75–89.
[14] Y.H. Su, C.-Y.A. Tsao, Modeling of solidification of molten metal droplet during atomization, Metall. Mater. Trans. B 28 (1997) 1249–1255.
[15] Y. Bayazitoglu, R. Cerny, Solidification of spherical metal drops in metal powder production, J. Mater. Processing Manufacturing Sci. 2 (1993) 51–61.
[16] C.M. Megaridis, Presolidification liquid metal droplet cooling under convective conditions, Atomization Sprays 3 (1993) 171–191.
[17] D. Turnbull, Formation of crystal nuclei in liquid metals, J. Appl. Phys. 21 (1950) 1022–1028.
[18] K.S. Dubey, P. Ramachandrarao, S. Lele, Thermodynamic properties of undercooled liquids, Int. J. Rapid Solidification 5 (1990) 221–228.
[19] D.P. Woodruff, The Solid–Liquid Interface, Cambridge University Press, London, UK, 1973 (Chapter 2).
[20] J.P. Hirth, Nucleation undercooling and homogeneous structures in rapidly solidified powders, Metall. Trans. A 9 (1978) 401–404.
[21] D. Turnbull, R.E. Cech, Microscopic observation of the solidification of small metal droplets, J. Appl. Phys. 21 (1950) 804–810.
[22] W.H. Hofmeister, M.B. Robinson, R.J. Bayuzick, Undercooling of pure metals in a containerless microgravity environment, Appl. Phys. Lett. 49 (1986) 1342–1344.
[23] G.D. Raithby, K.G.T. Hollands, Natural Convection, in: W.M. Rohsenow, J.P. Hartnett, E.N. Ganic (Eds.), Handbook of Heat Transfer Fundamental, McGraw-Hill, New York, 1985 (Chapter 6).
[24] K.F. Kelton, A.L. Greer, C.V. Thompson, Transient nucleation in condensed systems, J. Chem. Phys. 79 (1983) 6261–6272.
[25] Y.S. Touloukian, R.W. Powell, C.Y. Ho, P.G. Klemens, Thermophysical Properties of Matter, vol. 1, IFI/Plenum Data Corporation, New York, 1970.
[26] Y.S. Touloukian, E.H. Buyco, Thermophysical Properties of Matter, vol. 7, IFI/Plenum Data Corporation, New York, 1970.
[27] C.J. Simithells, E.A. Brandes, Metals Reference Book, fifth ed., Butterworths, London, UK, 1976.
[28] I. Barin, Thermochemical Data of Pure Substances, third ed., vols. 1–2, VCH, Weinheim, Germany, 1995.